THE JOURNAL OF BIOLOGICAL CHEMISTRY

Vol. 278, No. 47, Issue of November 21, pp. 46805–46813, 2003
*Printed in U.S.A.*

# Structural Basis for Tetrodotoxin-resistant Sodium Channel Binding by μ-Conotoxin SmIIIA*[S]

Received for publication, August 20, 2003, and in revised form, September 10, 2003
Published, JBC Papers in Press, September 10, 2003, DOI 10.1074/jbc.M309222200

**David W. Keizer‡, Peter J. West§¶, Erinna F. Lee‡, Doju Yoshikami¶, Baldomero M. Olivera¶, Grzegorz Bulaj¶‖, and Raymond S. Norton‡****

*From the ‡The Walter & Eliza Hall Institute of Medical Research, 1G Royal Parade, Parkville, Victoria 3050, Australia, §Interdepartmental Program in Neuroscience, University of Utah, Salt Lake City, Utah 84112, the ¶Department of Biology, University of Utah, Salt Lake City, Utah 84112, and ‖Cognetix Inc., Salt Lake City, Utah 84108*

**SmIIIA is a new μ-conotoxin isolated recently from *Conus stercusmuscarum*. Although it shares several biochemical characteristics with other μ-conotoxins (the arrangement of cysteine residues and a conserved arginine believed to interact with residues near the channel pore), it has several distinctive features, including the absence of hydroxyproline, and is the first specific antagonist of tetrodotoxin-resistant voltage-gated sodium channels to be characterized. It therefore represents a potentially useful tool to investigate the functional roles of these channels. We have determined the three-dimensional structure of SmIIIA in aqueous solution. Consistent with the absence of hydroxyprolines, SmIIIA adopts a single conformation with all peptide bonds in the *trans* configuration. The spatial orientations of several conserved Arg and Lys side chains, including $Arg^{14}$ (using a consensus numbering system), which plays a key role in sodium channel binding, are similar to those in other μ-conotoxins but the N-terminal regions differ, reflecting the *trans* conformation for the peptide bond preceding residue 8 in SmIIIA, as opposed to the *cis* conformation in μ-conotoxins GIIIA and GIIIB. Comparison of the surfaces of SmIIIA with other μ-conotoxins suggests that the affinity of SmIIIA for TTX-resistant channels is influenced by the $Trp^{15}$ side chain, which is unique to SmIIIA. $Arg^{17}$, which replaces Lys in the other μ-conotoxins, may also be important. Consistent with these inferences from the structure, assays of two chimeras of SmIIIA and PIIIA in which their N- and C-terminal halves were recombined, indicated that residues in the C-terminal half of SmIIIA confer affinity for tetrodotoxin-resistant sodium channels in the cell bodies of frog sympathetic neurons. SmIIIA and the chimera possessing the C-terminal half of SmIIIA also inhibit tetrodotoxin-resistant sodium channels in the postganglionic axons of sympathetic neurons, as indicated by their inhibition of C-neuron compound action potentials that persist in the presence of tetrodotoxin.**

Polypeptide toxins typically interact with their target receptors with high potency and exquisite selectivity and as such are valuable tools in elucidating the physiological functions of their targets and in probing the size and shape of their cognate binding sites. Toxins from the genus *Conus* have been especially valuable in this respect, and, of the various classes of conotoxin that have been characterized to date (1, 2), the μ-conotoxins represent a particularly good example. Their targets are the voltage-gated sodium channels (VGSCs),[1] which are responsible for the influx of sodium ions during action potentials in excitable tissues.

Three families of conotoxins target VGSCs, causing either inhibition (μ- and μO-conotoxins) or delayed inactivation (δ-conotoxins), but to date a detailed understanding of their interactions with the channel has been achieved only in the case of the μ-conotoxins. These toxins bind to Site 1 on VGSCs, one of several toxin binding sites identified on these channels (3). The pore-forming α-subunit of each VGSC consists of four homologous domains, each containing six putative transmembrane helices S1–S6, with the $Na^+$ channel thought to be formed by the S5-S6 loops from all four domains (these S5-S6 linkers are further subdivided into the S5-P, P, and P-S6 loops, with the P loop containing the SS1 and SS2 segments). Site 1, located on the extracellular surface of this pore, binds the guanidinium alkaloids tetrodotoxin (TTX) and saxitoxin as well as the μ-conotoxins. Not all VGSCs, however, bind TTX. Of the nine well characterized α-subunits cloned to date from mammals (4, 5), at least three, $Na_V1.5$, $Na_V1.8$, and $Na_V1.9$, can be classified as TTX-resistant. To probe the physiological roles of these VGSCs, and indeed of the different subtypes of TTX-sensitive VGSCs, additional blockers are needed. The μ-conotoxins offer considerable promise in this respect.

The first μ-conotoxin characterized, μ-conotoxin GIIIA from the fish-hunting snail *Conus geographus*, competes with TTX and saxitoxin for binding to Site 1 on the skeletal muscle $Na^+$ channel (6, 7) but is much more selective, targeting largely the skeletal muscle subtype $Na_V1.4$ (8). Of the neuronal subtypes studied thus far, $Na_V1.1$ is the most readily blocked by GIIIA, but the $EC_{50}$ is still an order of magnitude higher than that for $Na_V1.4$ (9). GIIIB, from the same species, has similar selectivity, binding preferentially to skeletal muscle over neuronal or cardiac subtypes (6, 7, 9–11). Another μ-conotoxin, PIIIA from the fish-hunting snail *Conus purpurascens*, also has a strong preference for the skeletal muscle subtype but can block other

* This work was supported in part by National Institute of General Medical Sciences Grant GM 48677 (to B. M. O.). The costs of publication of this article were defrayed in part by the payment of page charges. This article must therefore be hereby marked "*advertisement*" in accordance with 18 U.S.C. Section 1734 solely to indicate this fact.

[S] The on-line version of this article (available at http://www.jbc.org) contains Supplemental Fig. S1 and Tables SI–SIII.

** To whom correspondence should be addressed: The Walter & Eliza Hall Inst. of Medical Research, NMR Laboratory, 381 Royal Parade, Parkville, Victoria 3052, Australia. Tel.: 61-3-9903-9650; Fax: 61-3-9903-9655; E-mail: Ray.Norton@wehi.edu.au.

[1] The abbreviations used are: VGSC, voltage-gated sodium channel; GIIIA and GIIIB, μ-conotoxins GIIIA and GIIIB, respectively, from *C. geographus*; PIIIA, μ-conotoxin PIIIA from *C. purpurascens*; SmIIIA, μ-conotoxin SmIIIA from *C. stercusmuscarum*; Sm-P and P-Sm, chimeric μ-conotoxins; TTX, tetrodotoxin; CAP, compound action potential; TOCSY, total correlation spectroscopy; COSY, correlation spectroscopy; NOE, nuclear Overhauser effect; NOESY, nuclear Overhauser and exchange spectroscopy; r.m.s.d., root mean square deviation.

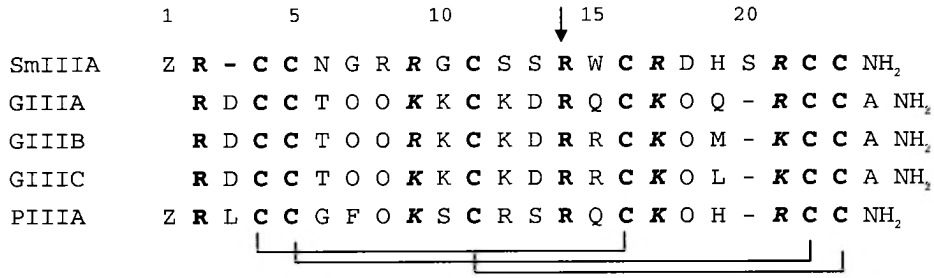


FIG. 1. **Amino acid sequences of SmIIIA, GIIIA, GIIIB, GIIIC, and PIIIA.** SmIIIA is from *C. stercusmuscarum*, GIIIA, GIIIB, and GIIIC are from *C. geographus* (Swiss-Prot accession numbers P01523, P01524, and P05482, respectively) and PIIIA is from *C. purpurascens* (Swiss-Prot accession number P58925). Note that a consensus numbering system has been adopted to encompass all μ-conotoxin sequences described to date. In the SmIIIA and PIIIA sequences, *Z* represents pyroglutamate. All peptides are C-terminally amidated. The locations of disulfide bonds previously determined in other μ-conotoxins are indicated, as well as the biologically important $Arg^{14}$. Cys and basic residues common to all sequences are in *bold*.

TTX-sensitive subtypes as well, albeit with lower affinity (8, 12, 13). Very recently, West *et al.* (14) described a novel μ-conotoxin, SmIIIA, from the fly speck cone snail *C. stercusmuscarum*, which blocked TTX-resistant VGSCs in frog sympathetic and dorsal root ganglia but had little effect on TTX-sensitive currents. SmIIIA thus represents the first specific antagonist for TTX-resistant $Na^+$ channels.

The amino acid sequence of SmIIIA is compared with those of GIIIA, GIIIB, GIIIC, and PIIIA in Fig. 1. The locations of the six half-cystines, and thus of three disulfide bridges, are conserved, as is the key residue $Arg^{14}$ (using the consensus numbering of Fig. 1). The important basic residues at positions 2, 9, 17, and 21 are also conserved or conservatively substituted. On the other hand, SmIIIA lacks the hydroxyproline residues found in all other μ-conotoxins described to date, contains a Trp at position 15 in contrast to Gln or Arg, and has an atypical sequence between the fourth and fifth half-cystines. As these changes might be expected to affect the three-dimensional structure of SmIIIA we have determined its structure in solution using NMR spectroscopic data. Comparison of the structure with those of GIIIA (15–17), GIIIB (18), and PIIIA (13) confirms that its overall fold and the spatial disposition of conserved Arg and Lys residues on the surface are similar but also allows some inferences to be drawn about the basis for the selectivity of SmIIIA for TTX-resistant channels. These inferences have been confirmed by the construction and assay of chimeras of SmIIIA and PIIIA in which the N- and C-terminal halves were recombined.

## EXPERIMENTAL PROCEDURES

*Peptide Synthesis and Sample Preparation*—Conotoxins SmIIIA and PIIIA and chimeras were synthesized, folded, and purified using the protocols described previously (12, 14). The peptides were purified using C18 reversed-phase HPLC and their identities confirmed by mass spectrometry.

Samples were prepared for NMR by dissolving SmIIIA in 350 μl of 95% $H_2O$/5% $^2H_2O$ to a final concentration of ~0.9 mM. The pH was adjusted to 4.7, but no buffer was present. pH was measured at room temperature and no allowances were made for isotope effects.

*NMR Spectroscopy*—Two-dimensional homonuclear TOCSY spectra with a spin-lock time of 50 ms and E-COSY spectra were collected on a Bruker AMX-500 spectrometer, and NOESY spectra with mixing times of 300, 200, and 75 ms were collected on a Bruker DRX-600 spectrometer, essentially as described previously (19). A 300-ms NOESY at pH 3.1 was also acquired. A series of one-dimensional spectra at 5 °C intervals were collected over the range 5–25 °C. Water was suppressed by use of the WATERGATE pulse sequence (20). Backbone amide exchange was measured by dissolving the sample in $^2H_2O$ at pH 4.4 and recording a series of one-dimensional and TOCSY spectra at 5 °C. Once exchange was complete, E-COSY and a 300-ms NOESY spectra were acquired. All amide proton signals except for $Cys^{16}$, $Arg^{17}$, and $Ser^{20}$ disappeared within 30 min, indicating that the protons were in fast exchange. The amide proton signals of $Cys^{16}$ and $Ser^{20}$ were still visible in a two-dimensional TOCSY acquired 4 h after $^2H_2O$ addition (Table SIII in Supplementary Material). A pH titration was performed over the range 1.5–9.5. All spectra were collected at 5 °C unless otherwise stated and were referenced to an impurity peak at 0.15 ppm or the water resonance. Spectra were processed using XWINNMR (Bruker Biospin) and analyzed using XEASY (21). Chemical shift assignments for SmIIIA have been deposited in the BioMagResBank data base (22).

*Structural Constraints*—SmIIIA contains three disulfide bonds linking the following pairs of half-cystines: $Cys^4$–$Cys^{16}$, $Cys^5$–$Cys^{22}$, and $Cys^{11}$–$Cys^{23}$. Appropriate restraints for each of these disulfides were included at each stage of the structure calculations. Distance restraints were obtained from the following spectra: 300- and 75-ms NOESY spectra at pH 4.7, 300-ms NOESY at pH 3.1, and 300-ms NOESY at pH 4.4 in $^2H_2O$, all acquired at 600 MHz. $^3J_{HNH\alpha}$ coupling constants were measured from a double quantum filtered COSY acquired at 500 MHz and then converted to dihedral restraints ($^3J_{HNH\alpha} > 8$ Hz, $\phi = -120 \pm 30°$; $^3J_{HNH\alpha} < 6$ Hz, $\phi = -60 \pm 30°$). If a positive $\phi$ angle could be excluded on the basis of NOE data (23), $\phi$ angles were restricted to the range −180 to 0°. $\chi_1$ angles were determined based on analysis of a 75-ms NOESY spectrum.

*Structure Calculations*—Two sets of structural calculations were performed in CYANA (24). Both used a set of four peak lists derived from the NOESY spectra described above. The first set of calculations used manual assignments for each peak. Intensities for each peak were calibrated using the conventional CALIBA script supplied with CYANA. These were then scaled by a factor of 1.2 before use in structural calculations to allow for possible effects of spin diffusion. A family of 200 structures was calculated using torsion angle dynamics, and 20 structures with the lowest target function were chosen for further analysis. No dihedral violations greater than 5° or NOE violations greater than 0.2 Å were observed in this family.

In addition to the traditional manual assignment of NOE cross peaks, we used the CANDID module of CYANA to assign NOE cross-peaks and calculate a structure for SmIIIA. The peak lists used for the manual assignments were supplied to CANDID and NOE assignments and structures were determined using the default scripts. The peak intensities from CANDID were equivalent to those obtained after scaling the peak intensities in the manually assigned peak lists by a factor of 1.2. Of the 1193 peaks supplied to CANDID, 1174 were assigned automatically, with the remainder being unassigned predominantly because of ambiguity among several possible assignments. Only eight of the assignments made by CANDID differed from those made manually. The backbone r.m.s.d. between structures calculated in CYANA using a manually assigned peak list and those calculated with the peak list produced by CANDID was 0.66, indicating that the methods were in excellent agreement.

The final NOE and dihedral restraint lists from CYANA were then used to calculate a family of 200 structures in Xplor-NIH (25) using the standard distance geometry and simulated annealing scripts. The library files supplied with Xplor-NIH were modified to include a pyroGlu residue. The lowest 30 structures in energy were chosen for further refinement. A water box was built around the molecule and then energy minimized on the basis of NOE and dihedral restraints and the geometry of bonds, angles, and impropers. A final family of 20 structures was then chosen for further analysis based on stereochemistry and energy considerations. This family has been deposited in the RCSB protein structural data base (Protein Data Base accession number 1Q2J). Structures were analyzed using the programs PROCHECK (26) and MOLMOL (27). Structural figures were prepared using MOLMOL (27),

GRASP (28), and InsightII (Accelrys, San Diego, CA).

*Dissociated Neuron Preparation*—Lumbar paravertebral ganglia 8–10 were dissected from 6–7.5-cm adult frogs (*Rana pipiens*) of either sex and processed as described previously (29, 30). Briefly, ganglia were treated with collagenase followed by trypsin. Cells were mechanically dissociated by trituration, washed, and suspended in 73% Leibowitz's L15 solution (supplemented with 14 mM glucose, 1 mM $CaCl_2$, 7% fetal bovine serum, and penicillin/streptomycin), plated on polylysine-coated coverslips, and stored at 4 °C.

*Whole Cell Patch Clamp Electrophysiology*—Whole cell patch clamp recordings were made essentially as described previously (14). Briefly, sympathetic neurons were perfused with extracellular solution containing (in mM): NaCl, 117; KCl, 2; $MgCl_2$, 2; $MnCl_2$, 2; HEPES, 5; TEA, 10; TTX, 0.01; pH 7.2. Recording pipettes contained (in mM): NaCl, 10; CsCl, 110; $MgCl_2$, 2; $CaCl_2$, 0.4; EGTA, 4.4; HEPES, 5; TEA, 5; MgATP, 4; pH 7.2. These solutions inhibit voltage-gated $K^+$, $Ca^{2+}$, and TTX-sensitive $Na^+$ currents, thereby permitting recording of TTX-resistant $Na^+$ currents exclusively. Conotoxins were dissolved in extracellular solution and applied to neurons by bath exchange. Toxin exposures were conducted in static baths. To evoke voltage-gated TTX-resistant $Na^+$ currents, the neuron was held at −80 mV, while 50-ms test pulses to 0 mV were applied every 10 s. Each test pulse was preceded by a −120 mV prepulse lasting 50 ms to relieve steady-state inactivation. Current signals, acquired at room temperature with an Axopatch 200B amplifier (Axon Instruments), were filtered at 2 kHz, digitized at 10 kHz, and leak-subtracted by a P/5 protocol using in-house software written in LabVIEW (National Instruments, Austin, TX).

*Extracellular Electrophysiology*—Extracellular recordings of compound action potentials (CAPs) in sympathetic nerves were made essentially as described previously (31). Briefly, lumbar paravertebral ganglia 8–10 and the adjoining 10th spinal nerve were dissected from 6–7.5 cm adult frogs (*R. pipiens*) of either sex. The recording chamber was fabricated from Sylgard and consisted of seven circular or semicircular compartments with diameters of 4–5 cm (see Fig. 4*A*), each separated from its neighbor by a partition about 1-mm wide. A bead of Vaseline was placed atop each partition between compartments. The chain of sympathetic ganglia and attached 10th nerve were arranged in the compartments as illustrated in Fig. 4*A*. Those portions draped over the Vaseline-topped partitions were covered with additional Vaseline to prevent drying and to seal compartments from each other such that the fluid in each compartment was isolated and independently maintained and electrical stimulation or recording across compartment partitions was possible. Each compartment was maintained essentially as a static bath except for the test compartment, which was perfused when it did not contain toxin. All compartments contained normal frog Ringer's solution consisting of (in mM): NaCl, 111; KCl, 2; $CaCl_2$, 1.8; HEPES, 10; pH 7.2. Conotoxins were dissolved in this solution and applied to the test compartment by stopping its perfusion and replacing the solution with one containing toxin. During toxin exposure, the test compartment was static to conserve toxin.

Platinum wire electrodes were used to convey supramaximal stimuli to the preganglionic sympathetic chain between the 8th and 9th ganglia and to record postganglionic CAPs in the 10th spinal nerve. Stimuli (0.1–1-ms rectangular voltage pulses) were provided by a stimulator (S-88, Grass Instruments) through a stimulus isolation unit. Recordings were made using a differential A/C preamplifier (P-55, Grass Instruments, with bandpass filter settings of 1 Hz and 1 kHz). All experiments were performed at room temperature.

## RESULTS

*NMR Spectroscopy*—Broad NH chemical shift dispersion in one-dimensional spectra indicated that SmIIIA was well structured, and two-dimensional homonuclear spectra recorded at 5, 15, and 25 °C showed that only one conformation was present in aqueous solution at these temperatures. Sequence-specific resonance assignments for backbone and side-chain protons in SmIIIA were made at 500 and 600 MHz using standard two-dimensional homonuclear NMR experiments. Assignments at pH 4.7 and 3.1 are tabulated in Supplementary Material and have been deposited with BioMagResBank (22) with accession number 5881. Distance constraints were taken from the volumes of NOE cross-peaks in NOESY spectra acquired at 5 °C at 600 MHz.

*NMR Assessment of Hydrogen Bonds*—The temperature dependence of each amide proton chemical shift was determined to probe for hydrogen bonding. The amide protons of $Cys^5$, $Gly^{10}$, $Cys^{11}$, $Cys^{16}$, $Arg^{17}$, $His^{19}$, $Ser^{20}$, and $Cys^{23}$ exhibited temperature coefficients of magnitude ≤4 ppb/°C (see Supplementary Material), consistent with their possible involvement in hydrogen bonds (32). However, amide exchange experiments conducted at 5 °C and pH 4.4 indicated that all amide protons, except for those of $Cys^{16}$ and $Ser^{20}$, exchanged with solvent deuterium within minutes of dissolution of the polypeptide in $^2H_2O$. Amide protons from these residues were apparent in NMR spectra for several hours following dissolution. Because even the most slowly exchanging amides in SmIIIA exchanged relatively quickly, no hydrogen bonds were used as distance constraints in the structure calculations.

TABLE I
*Structural statistics for SmIIIA*

| | |
|---|---|
| Distance restraints | 224 |
| Intra ($i = j$) | 34 |
| Sequential ($\|i - j\| = 1$) | 67 |
| Short ($1 < \|i - j\| < 6$) | 91 |
| Long | 32 |
| Dihedral restraints | 30 |
| Energies (kcal $mol^{-1}$)[a] | |
| $E_{NOE}$ | 3.6 ± 0.6 |
| Deviations from ideal geometry[b] | |
| Bonds (Å) | 0.0034 ± 0.0001 |
| Angles (°) | 0.618 ± 0.008 |
| Impropers (°) | 0.442 ± 0.009 |
| r.m.s.d. (Å)[c] | |
| All heavy atoms | 1.98 |
| Backbone heavy atoms (N, $C^\alpha$, C′) | 0.77 |
| Ramachandran plot[d] | |
| Most favored (%) | 66.7 |
| Allowed (%) | 29.4 |
| Additionally allowed (%) | 3.9 |
| Disallowed (%) | 0 |

[a] The values for $E_{NOE}$ are calculated from a square well potential with force constants of 50 kcal $mol^{-1}$ $Å^2$.
[b] The values for the bonds, angles, and impropers show the deviations from ideal values based on perfect stereochemistry.
[c] r.m.s.d. over all residues.
[d] As determined by the program PROCHECK-NMR for all residues except Gly and Pro (26).

*Solution Structure*—Parameters characterizing the final 20 structures of SmIIIA and structural statistics are summarized in Table I, and stereo views of the structures superimposed over the backbone are shown in Fig. 2. Inspection of Table I indicates that the final 20 structures fit well with experimentally derived distance and angle constraints and are well defined over the entire length of the polypeptide. The structures of SmIIIA have been deposited with the RSCB Protein Data Bank (accession number 1Q2J) (33).

The angular order parameters, $S$, for the backbone $\phi$ and $\psi$ angles and the side-chain $\chi^1$ angles of SmIIIA are presented in Fig. S1 in the Supplementary Material. The $\phi$ and $\psi$ angles are well ordered ($S_{\phi,\psi} > 0.9$) for all residues except $Arg^8$, for which $S_\psi$ is 0.82, indicating that the structure is well defined. Of the three disulfide bridges in SmIIIA, two, $Cys^4$–$Cys^{16}$ and $Cys^5$–$Cys^{22}$ have a left-handed ($\chi^{SS}$ −90°) configuration and $Cys^{11}$–$Cys^{23}$ is right-handed ($\chi^{SS}$ +90°).

In the N-terminal region of SmIIIA the pattern of NOEs and hydrogen bonds is consistent with a series of turns, including an inverse γ-turn at $Cys^4$ and a γ-turn at $Gly^{10}$. There is no evidence of the β-hairpin seen in the N-terminal region of GIIIB (18). The backbone between $Ser^{13}$ and $Ser^{20}$ adopts a distorted helical structure, with an $i + 2$ to $i$ hydrogen bond from $Arg^{17}$ to $Trp^{15}$ implying a $3_{10}$- rather than an α-helical character, but this does not continue through to the C terminus. In its lack of a β-hairpin in the N-terminal region and limited helical character in the C-terminal half, SmIIIA appears to be more similar to PIIIA (13) than GIIIB. However,

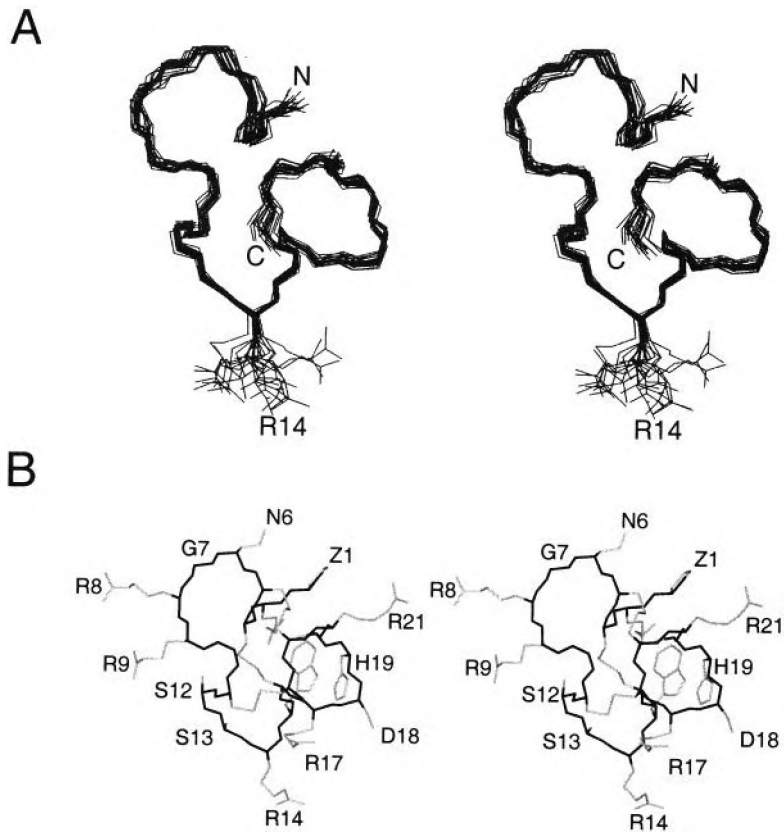


FIG. 2. **SmIIIA structure.** *A*, stereo views of the family of 20 final structures determined for SmIIIA, superimposed over backbone heavy (N, $C^{\alpha}$, C′) atoms from all 22 residues. For clarity, only the side chain of the biologically important $Arg^{14}$ is shown. The letters *N* and *C* refer to the amino and carboxyl termini, respectively. *B*, stereo view of the closest-to-average structure in the family shown in *A*, showing the backbone (*black*) and side chains (*gray*).

when we subjected the structures of GIIIB to analysis in PROCHECK (26) little secondary structure was predicted, with only a turn of helix over residues $Arg^{14}$ to $Cys^{16}$ and $Lys^{21}$ to $Cys^{23}$ being present in 4 out of 20 structures in Protein Data Bank entry 1GIB. In fact, the backbone of SmIIIA over residues 11–17 overlays with the corresponding region of GIIIB with an r.m.s.d. of 1.00 Å (1.07 Å in the case of GIIIA), indicating that the structures are quite similar despite the different descriptions of their ordered secondary structure. By contrast, when the N-terminal region is included, the r.m.s.d. values are 2.46 and 3.00 Å to GIIIB and GIIIA, respectively, confirming that there are significant differences between SmIIIA and GIIIA/B in this region, as was the case for PIIIA. r.m.s.d. values to PIIIA cannot be calculated because the PIIIA structure has not been deposited with the Protein Data Bank.

SmIIIA is a highly basic polypeptide as a consequence of its 6 Arg residues. The only other charged side chains are those of $Asp^{18}$ and $His^{19}$, and both the N and C termini are blocked. As illustrated in Fig. 3, the surface of SmIIIA is highly positively charged, relieved only by the negatively charged $Asp^{18}$ on one face. The indole ring of $Trp^{15}$, which is unique to SmIIIA, is flanked by the imidazolium ring of $His^{19}$ on one side and the guanidinium moiety of $Arg^{2}$ on the other (Fig. 2). These side chain interactions would be favored not only by interactions between the $\pi$ orbitals of the indole and imidazolium rings but also by aromatic-cation interactions (34). Interestingly, the relative orientation of Trp and Arg side chains in SmIIIA shows some similarity to those of the Trp and Arg side chains in the "WSWX" structures of hemopoietic cytokine receptors, such as that for erythropoietin (35). Analysis of ring current shifts in the final structures was performed in MOLMOL using both the Johnson-Bovey and Haigh-Mallion methods (27, 36). As a consequence of the close proximity of $His^{19}$ and $Arg^{2}$ to the indole ring, resonances of both are perturbed by ring current effects, with deviations upfield of more than 0.5 ppm predicted for $C^{\beta}H$, $C^{\gamma}H$, and $C^{\delta}H$ of $Arg^{2}$ and $C^{\alpha}H$, $C^{\beta}H$, and ring protons of $His^{19}$. The $C^{\epsilon}H$ resonance of $His^{19}$ is shifted upfield significantly, but in $Arg^{2}$ only the $C^{\delta}H_2$ resonance is shifted, and by only 0.2 ppm compared with other Arg side chains, perhaps reflecting some flexibility in the $Arg^{2}$ position.

*pH Dependence*—A limited pH titration was undertaken to determine the $pK_a$ values for the $Asp^{18}$ carboxyl and $His^{19}$ imidazolium groups. The $Asp^{18}$ $pK_a$ of 3.8 is very similar to that of the carboxyl group of Asp in small peptides, *viz.* 3.9 (37, 38). In small histidine-containing peptides the imidazolium $pK_a$ was 7.0 at 35 °C (38), while in the uncharged model compound Ac-His-NHMe it was 6.38 at 37 °C (39), 6.43 in $H_2O$, and 6.54 in $^2H_2O$, each containing 0.1 M NaCl at 30 °C (40). The intrinsic $pK_a$ cited by Shire *et al.* (41) is 6.3. The $His^{19}$ $pK_a$ of 6.8 is slightly higher than the model values. Given the highly basic nature of SmIIIA, a reduced $pK_a$ might have been expected for $His^{19}$, but these influences must be offset by proximity of the imidazolium ring to the negatively charged side chain of $Asp^{18}$ and by cation-aromatic interactions with the indole ring of $Trp^{15}$, both of which would tend to stabilize the imidazolium form.

*Minor Conformers and Conformational Averaging*—Previous NMR studies of μ-conotoxins have found evidence of conformational flexibility, manifested in line broadening of one or more resonances (15, 17, 18). By contrast, no significant line broadening was observed for SmIIIA at pH 4.7 or 3.1 over the temperature range 5–25 °C, from which we infer that SmIIIA does not undergo significant conformational averaging in aqueous solution.

Minor peaks with intensities ≤10% of the main peaks were present in spectra of SmIIIA but may have arisen from impurities in the synthetic sample used for structure determination (although its purity was >95% according to reversed-phase HPLC). Moreover, analysis of backbone NOEs confirms that all peptide bonds in SmIIIA adopt the *trans* conformation. This contrasts with the behavior of other μ-conotoxins investigated by NMR, where multiple conformations associated with *cis*-

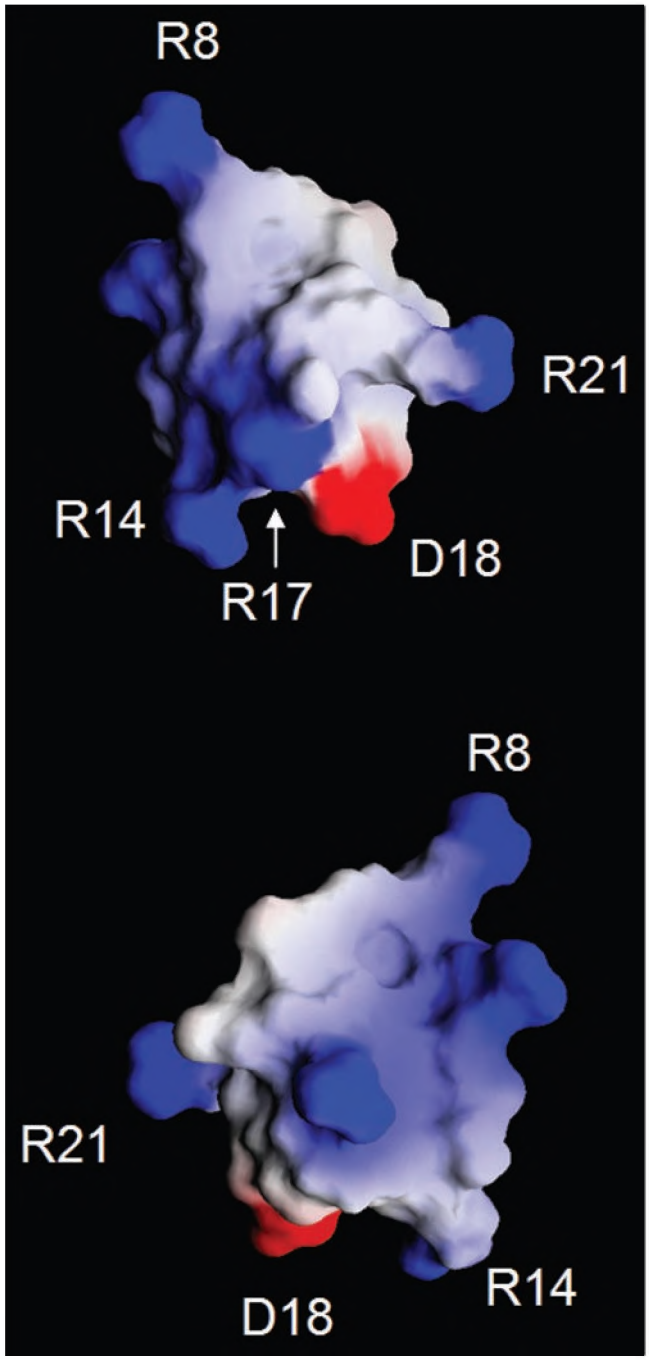


FIG. 3. **Surface representation of SmIIIA.** The surface is colored, with basic residues in *blue* and acidic residues in *red*. The two views in *A* and *B* are related by a 180° rotation around the *vertical axis*. This figure was prepared using GRASP (28).

*trans* isomerism have been observed. In PIIIA the ratio of major to minor conformer was about 3:1 (13). Minor conformers associated with *cis-trans* isomerism were not noted for GIIIB by Hill *et al.* (18), although there is a statement by Nielsen *et al.* (13) that minor (*trans*) conformers of GIIIA and GIIIB were "masked by broadening associated with intermediate exchange occurring on the NMR time scale."

*Electrophysiological Analysis of μ-Conotoxins and Chimeras*—Unlike SmIIIA, μ-conotoxin PIIIA does not inhibit TTX-resistant VGSCs in rat DRG neurons (13) or in frog sympathetic neurons (Fig. 4*A*). To test the hypothesis that residues in the C-terminal half of SmIIIA determine affinity for TTX-resistant VGSCs, two complementary chimeras of SmIIIA and PIIIA were generated (Table II). The C-terminal half of SmIIIA, beginning at $Arg^{14}$, was replaced by the corresponding PIIIA residues in μ-chimera Sm-P, while in the second, P-Sm, the C-terminal half of PIIIA was replaced by the corresponding SmIIIA residues.

Although SmIIIA inhibits TTX-resistant VGSCs with minimal effects on TTX-sensitive VGSCs in frog sympathetic neurons (14), it does inhibit CAPs in frog skeletal muscle (summarized in Table II; data not shown). Inhibition by SmIIIA of muscle CAPs is reversed by washing, unlike the irreversible inhibition by PIIIA (12). In contrast, SmIIIA inhibition of TTX-resistant VGSCs in frog sympathetic and DRG neurons is essentially irreversible (14), indicating that its affinity for these VGSCs is greater than its affinity for those in frog skeletal muscle. Since both PIIIA and SmIIIA inhibit CAPs in frog skeletal muscle, this tissue was used to assess the baseline activities of the Sm-P and P-Sm chimeras. As summarized in Table II, both chimeras reversibly inhibited muscle CAPs, indicating that the structures of these peptides resembled those of their parent compounds to the extent that they retained their biological activities.

The effects of the chimeric μ-conotoxins on TTX-resistant VGSCs were compared on voltage-clamped frog sympathetic neurons (Fig. 5). Neurons were held at −80 mV, and 50-ms test pulses to 0 mV were applied at 0.1 Hz. Each test pulse was immediately preceded by a 50 ms prepulse to −120 mV (see voltage-command protocol diagrammed at the *top* of Fig. 5) to relieve any steady-state inactivation that may have occurred at the −80 mV holding potential. The beginning of the test pulse is indicated by an *arrow* both in the voltage-command diagram and in the current response traces. All illustrated responses in the presence of toxin represent those obtained only after the preparation had equilibrated with peptide for >10 min.

Although 1 μM PIIIA does not inhibit TTX-resistant currents in these neurons (Fig. 5*A*), 1 μM SmIIIA irreversibly inhibited nearly all of the TTX-resistant current (Fig. 5*B*), verifying our previous findings (14). Like PIIIA, 1 μM Sm-P did not inhibit TTX-resistant currents (Fig. 5C). In contrast, 1 μM P-Sm (the "inverse" chimera) did inhibit the TTX-resistant current in a manner similar to that of SmIIIA (Fig. 5*D*). As seen in the *bottom half* of Fig. 5*D*, the time course of this inhibition was slower than that of native SmIIIA, and complete inhibition was not achieved during the 20-min toxin exposure in this experiment. Nevertheless, the inhibition was not reversed when the preparation was perfused with toxin-free bathing solution for 30 min, indicating that the P-Sm chimera, like SmIIIA, has a high affinity for TTX-resistant VGSCs in these neurons.

To further characterize the activity of these peptides, CAPs were recorded from sympathetic postganglionic axons in the 10th spinal nerve essentially as described previously (31). These CAPs were evoked by stimulating the preganglionic axons in the sympathetic chain (Fig. 4*A*). The sympathetic ganglia contain two populations of physiologically and pharmacologically distinct neurons: the B- and C-neurons. Due to differences in axon diameter and myelination, B-neurons have faster conducting pre- and postganglionic axons than those of C-neurons (for review, see Ref. 42). These differences in action potential conduction velocity are manifested by differences in CAP latency (Fig. 4*B*, *Control*). The CAP with shortest latency corresponds to the "fast B-neurons", whose pre- and postganglionic axons are both myelinated. The CAP with the longest latency corresponds to the "C-neurons," whose pre- and postganglionic axons are both non-myelinated. The small CAP with intermediate latency corresponds to the "slow B-neurons," which have myelinated preganglionic axons and non-myelinated postganglionic axons.

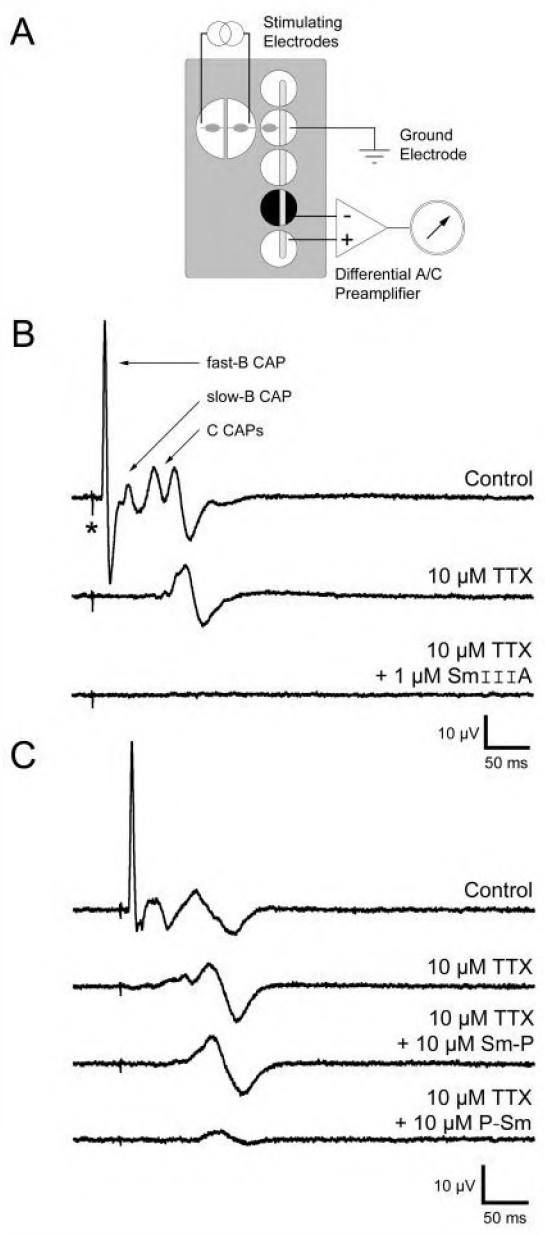


FIG. 4. **Both SmIIIA and μ-chimera P-Sm inhibit C-neuron CAPs that persist in the presence of TTX.** *A*, sketch of preparation, recording chamber, and arrangement of stimulating and recording electrodes. Supramaximal stimuli were applied to the connective between the 8th and 9th ganglia to excite the preganglionic nerve innervating the 10th ganglion. CAPs in the postganglionic axons of neurons of the 10th ganglion were recorded from the 10th spinal nerve. Toxins were applied at the indicated concentrations in the test compartment (darkened well) that contained a segment of the 10th spinal nerve as well as the negative lead of the differential A/C preamplifier. Thus, only postganglionic axons were exposed to toxins. *B*, representative traces of CAPs in the presence of 10 μM TTX or 10 μM TTX + 1 μM SmIIIA compared with a control trace. Each trace represents the average of 10 responses. The *asterisk* indicates the stimulus artifact. Note that C-neuron CAPs were not inhibited by 10 μM TTX, indicating that the expression level of TTX-resistant VGSCs was sufficient to propagate action potentials in these axons when only these channels remained active. However, when 1 μM SmIIIA was present in addition to TTX, C-neuron CAPs were inhibited, indicating that SmIIIA inhibits TTX-resistant VGSCs. *C*, recordings of CAPs before (control) and in the presence of 10 μM TTX, 10 μM TTX + 10 μM Sm-P, or 10 μM TTX + 10 μM P-Sm. Each trace represents the average of 10 responses. As in *B*, C-neuron CAPs were not inhibited by 10 μM TTX. Sm-P did not inhibit the C-neuron CAP that persisted in TTX. In contrast, P-Sm did inhibit the C-neuron CAP, indicating that P-Sm inhibits TTX-resistant VGSCs in the postganglionic axons of sympathetic C-neurons in a manner similar to that of SmIIIA.

TABLE II
*Sequences and activities of SmIIIA and PIIIA and chimeric μ-conotoxins Sm-P and P-Sm*

| | | Inhibition of frog muscle CAP (1 μM)[a] |
|---|---|---|
| Native μ-conotoxins | | |
| SmIIIA | ZR-CCNGRRGCSSRWCRDHSRCC | + |
| PIIIA | ZRLCCGFOKSCRSRQCKOH-RCC | + |
| μ-Conotoxin chimeras | | |
| Sm-P[b] | **ZR-CCNGRRGCSS**RQCKOH-RCC | + |
| P-Sm[b] | ZRLCCGFOKSCRS**RWCRDHSRCC** | + |

[a] All of these peptides are able to inhibit the CAP in frog skeletal muscle. Thus, the chimeras retain biological activity as determined by this assay.
[b] Residues belonging to SmIIIA and PIIIA are in bold and standard font, respectively.

When 10 μM TTX was applied to postganglionic axons in this preparation, fast B-neuron and slow B-neuron CAPs were inhibited, while C-neuron CAPs were spared (Fig. 4*B*, 10 μM TTX). This indicates that sympathetic C-neurons express sufficient levels of TTX-resistant VGSCs in their axons to allow action potential propagation, albeit at a slower conduction velocity (note latency difference of C-CAPs in control *versus* TTX-treated preparations in Fig. 4). Since SmIIIA inhibits TTX-resistant VGSCs, it was predicted that SmIIIA would also inhibit C-neuron CAPs that persist in 10 μM TTX. Indeed, as seen in Fig. 4*B* (10 μM TTX + 1 μM SmIIIA), application of 1 μM SmIIIA did inhibit the C-neuron CAP that persisted in 10 μM TTX. This inhibition did not reverse when the preparation was perfused with bathing solution containing only TTX (not shown), consistent with the irreversible activity of SmIIIA on TTX-resistant currents.

In Fig. 4*C*, the Sm-P and P-Sm μ-chimeras were tested for their ability to inhibit C-neuron CAPs that persist in TTX. As in Fig. 4*B*, only the C-neuron CAP remained after exposing the preparation to 10 μM TTX. When 10 μM Sm-P was added, the C-neuron CAP remained largely unaltered (Fig. 4*C*, 10 μM TTX + 10 μM Sm-P). In contrast, when 10 μM P-Sm was added to the same preparation, the C-neuron CAP was inhibited (Fig. 4*C*, 10 μM TTX + 10 μM P-Sm). This indicates that the P-Sm chimera, but not the Sm-P chimera, inhibits TTX-resistant VGSCs expressed in the axons of sympathetic C-neurons, in agreement with the voltage-clamp results presented in Fig. 5.

## DISCUSSION

SmIIIA blocks TTX-resistant channels whereas GIIIA, GIIIB, GIIIC, and PIIIA block various categories of TTX-sensitive channels. It is instructive to compare their solution structures to ascertain the extent to which these different subtype specificities are reflected in structural differences as opposed simply to different side chains displayed on similar scaffolds. In making this comparison we have used the consensus numbering system presented in Fig. 1. The major structural features of GIIIB (18) were described as a distorted helix from residues 14–24 (using the consensus numbering of Fig. 1) and a small β-hairpin involving residues 4–10, with a turn centered around residues 7–8. A type I β-turn is centered on $Cys^4$-$Cys^5$, although this coincides with the first segment of the β-hairpin and is somewhat distorted. A second turn involving residues 6–9 is located in the β-hairpin, but it does not fit any of the standard turn types, no doubt partly because of the presence of *trans*-$Hyp^7$ and *cis*-$Hyp^8$. A third turn involving residues 10–13 joins the β-hairpin to the helix but low backbone angular order parameters for this region imply that it accesses more than one conformation.

Hill *et al.* (18) also made a detailed comparison of the structure of GIIIB with previously reported structures of GIIIA.

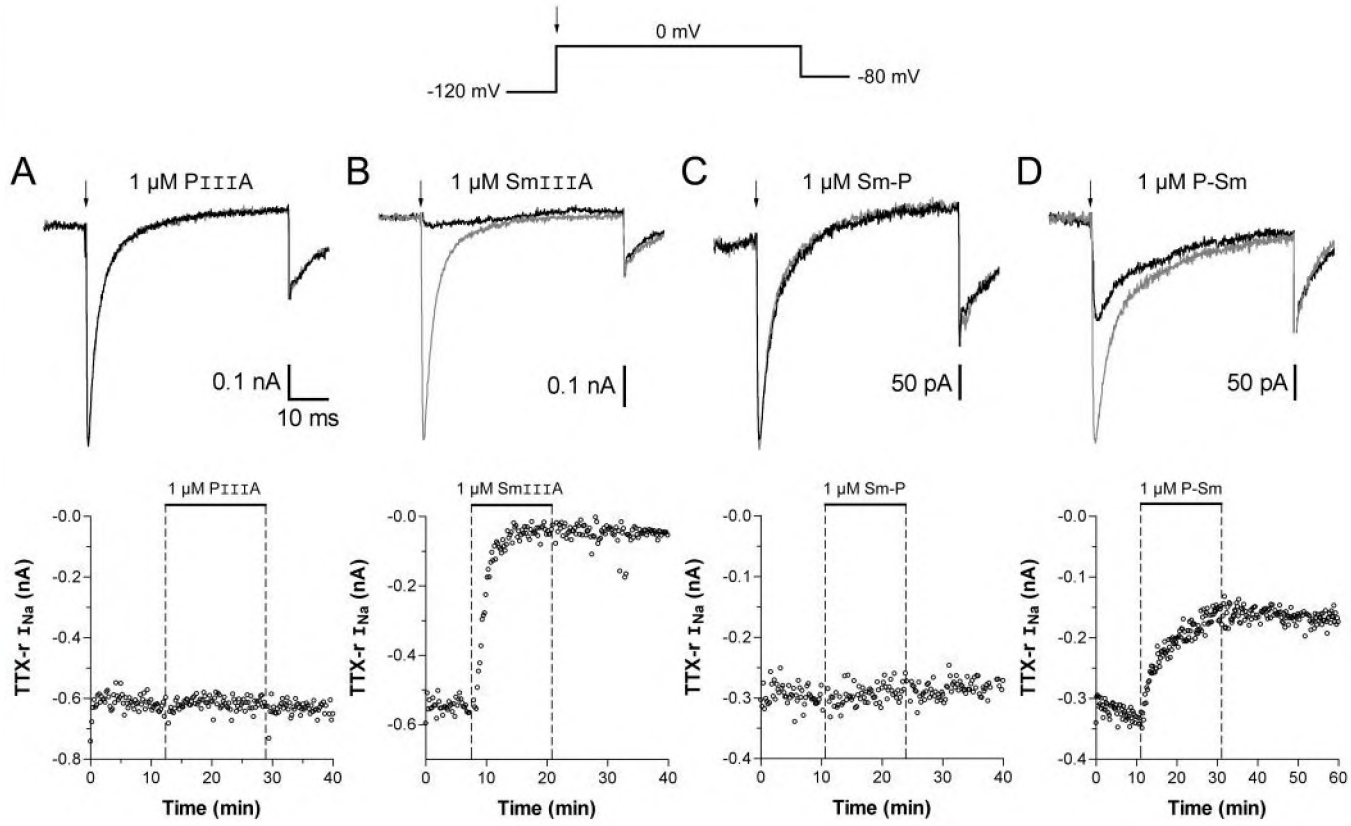


FIG. 5. **Comparison of native and chimeric μ-conotoxin effects on TTX-resistant sodium currents.** The voltage-command protocol is shown at the *top*. Neurons were held at −80 mV, and a 50-ms test pulse to 0 mV was used. Each test pulse was preceded by a 50-ms prepulse to −120 mV to relieve steady-state inactivation. The beginning of the test pulse is indicated by an *arrow*. *A–D*, representative recordings in the presence of PIIIA (*A*), SmIIIA (*B*), chimera Sm-P (*C*), or chimera P-Sm (*D*). All neurons were exposed to 1 μM toxin for no less than 10 min. The *top half* of each panel shows the average of 10 current traces in the presence of toxin as compared with matching controls (*gray*). Time calibration *bar* shown in *A* applies to all. *Arrows* indicate the beginning of the test pulse (see also the *arrow* in the voltage-command protocol diagram). The *bottom half* of each panel shows the peak amplitudes of the TTX-resistant currents plotted as a function of time. In all experiments, 10 μM TTX was present throughout. Data were taken from traces evoked by test pulses applied every 10 s. *Horizontal black bars* flanked by *dashed vertical lines* indicate when toxin was present. Note that P-Sm, like SmIIIA, irreversibly inhibited the TTX-resistant sodium current. In contrast, neither PIIIA nor Sm-P inhibited the TTX-resistant sodium current.

GIIIA (15–17) was described as consisting of β-turns ($Asp^3$–$Thr^6$ and $Thr^6$–$Lys^9$), a linear extension ($Lys^9$–$Asp^{13}$), a non-hydrogen-bonded loop ($Asp^{13}$–$Cys^{16}$), and a single right-handed helical turn ($Cys^{16}$–$Gln^{19}$), with a final loop directing the C terminus away from the core in the opposite direction to the N terminus. By contrast, GIIIB was described as containing a small β-hairpin involving residues 4–10 and $3_{10}$-helix from residues 14–24. In fact, the backbones of the two structures superimpose quite well (r.m.s.d. 1.36 Å) and the differences between them lie more in the descriptions of the structures than the structures themselves.

Very recently, Nielsen *et al.* (13) determined the solution structure of PIIIA. As this μ-conotoxin is able to block $Na_V1.4$, many of the structural features in GIIIA and GIIIB are likely to be conserved in PIIIA, although some structural differences might be expected to account for the high affinity of PIIIA for both neuronal and muscle forms of TTX-sensitive VGSCs. Although the C-terminal regions of PIIIA and GIIIA overlap and the functionally important $Arg^{14}$ is exposed in a similar manner, marked differences are apparent in the orientation of the N-terminal region to the end of loop 1 at $Cys^{11}$. The distorted β-hairpin in GIIIB and possibly GIIIA was replaced in the major conformation of PIIIA by a series of loops, reflecting the presence of a *trans* conformation at $Hyp^8$ in the major conformer of PIIIA in contrast to the *cis* conformation in GIIIA and GIIIB, as discussed above. This affects the locations of residues such as $Arg^2$ and $Lys^9$, which are moderately important for GIIIA binding to the $Na^+$ channel. Effects of *cis-trans* isomerization on the C-terminal region of PIIIA are minimal, however, with the orientations of functionally important residues such as $Arg^{14}$, $Lys^{17}$, and $Arg^{20}$ being similar to those of their GIIIA counterparts.

In fact, we believe that the C-terminal halves of all of these μ-conotoxins have similar structures despite the different descriptions in the literature. By contrast, the N-terminal regions do differ, reflecting the *trans* conformation for the peptide bond preceding residue 8 in SmIIIA and the major form of PIIIA, as opposed to the *cis* conformation in GIIIA, GIIIB, and the minor form of PIIIA. Taking into account these structural differences and differences in amino acid sequence, how do the surfaces these toxins present to the $Na^+$ channel differ? Fig. 6 compares two views of the surface of SmIIIA with the corresponding surfaces of GIIIA and GIIIB. The disulfide bridges (shown in *yellow*) are conserved across the three structures but their surface exposure varies slightly according to the position of surface loops and side chains. Of the basic residues, 5 ($Arg^2$, $Arg/Lys^9$, $Arg^{14}$, $Arg/Lys^{17}$, and $Arg/Lys^{21}$) are conserved, SmIIIA has an additional Arg at position 8, GIIIA and GIIIB have an additional Lys at positions 10 and 12, and GIIIB has an Arg at position 15 (Fig. 1). The *upper part* of Fig. 6 shows that the orientations of $Arg^{14}$ and $Arg/Lys^{21}$ are conserved across all three structures, and the *lower half* shows that this is also true for $Arg/Lys^{17}$ (where this side chain is adjacent to $Arg^{14}$ and pointing toward the viewer). By contrast, $Arg/Lys^9$ is oriented quite differently in SmIIIA compared with GIIIA and

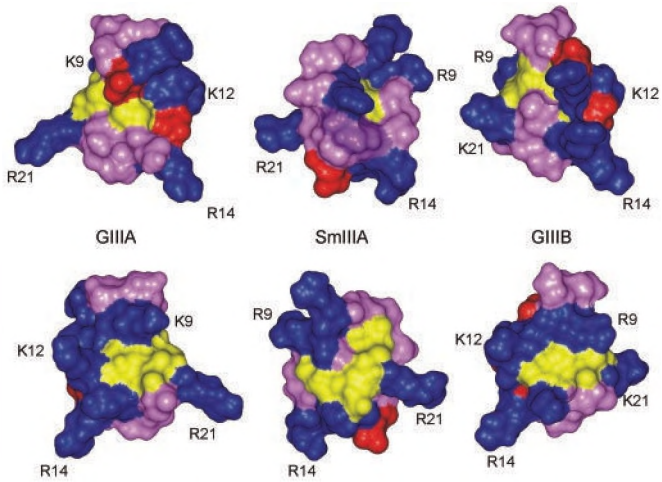


FIG. 6. **CPK surface representations of SmIIIA (*center*; Protein Data Bank accession number 1Q2J) compared with GIIIA (*left*; Protein Data Bank accession number 1GIB) and GIIIB (*right*; Protein Data Bank accession number 1TCG).** Arg and Lys residues are colored *dark blue*, Asp *red*, Cys *yellow*, and all others *pink*, except for the $Trp^{15}$ side chain of SmIIIA, which is shown in *magenta*. This figure was prepared using InsightII (Accelrys).

GIIIB, as evident in the lower view in Fig. 6, and $Arg^2$ is located just above $Trp^{15}$ in SmIIIA but near $Lys^{10}$ in GIIIA and GIIIB (which is in turn near $Lys^{12}$). In these respects, SmIIIA appears to be more similar to the major form of PIIIA than to GIIIA or GIIIB, although a detailed comparison of these structures is not possible because the PIIIA structure is not available. These similarities reflect the different orientation of the N terminus in SmIIIA arising from the *trans* conformation for the peptide bond preceding residue 8. $Asp^3$ and $Asp^{13}$ of GIIIA and GIIIB occupy different positions in the sequence and on the surface compared with $Asp^{18}$ of SmIIIA. Given their proximity to $Arg^{14}$ and their different locations relative to this key side chain, they could be expected to influence sodium channel binding.

In addition to these differences in the locations of charged side chains, there are also differences in shape between SmIIIA and GIIIA/GIIIB, particularly at the top of the structure as viewed in Fig. 6. Again, these reflect the different orientation of the N terminus in SmIIIA. $Ser^{13}$ is buried in PIIIA, consistent with it playing a structural role that ensures the exposure of $Arg^{14}$ (13). In SmIIIA, $Ser^{12}$ and $Ser^{13}$ are located on the surface of the protein, and the side chain of $Ser^{13}$ is involved in a hydrogen bond. The $O^{\gamma}H$ resonances of both of these residues are exchanging slowly enough with solvent to be resolved in the spectrum, indicative of some protection from solvent. Analysis of solvent accessibility shows that most backbone amides are shielded from solvent but when the accessibility of entire residues is considered, $Cys^4$, $Gly^{10}$, $Cys^{16}$, and $Ser^{20}$ stand out as being the least exposed.

Mutational analysis of GIIIA shows that $Arg^{14}$ is a particularly important residue for binding as well as for blockade of channel function (43–45). When the toxin is bound, $Arg^{14}$ appears to occupy the mouth of the channel and inhibits $Na^+$ flux by acting as both a steric and electrostatic barrier (46–48). The GIIIA mutant R14Q binds with poor affinity and when bound reduces channel conductance by only 70% compared with the native toxin which blocks conductance 100% (44); this has been taken to indicate that the toxin binds to the pore with $Arg^{14}$ very close to the selectivity filter. Replacement of numerous other residues of the toxin also affects its function, indicating that many parts of the toxin surface interact with the $Na^+$ channel (49). Charges grouped on one side of the toxin at positions 2, 13, and 15 had a weaker influence, whereas residue 17, on the opposite face, was more important. It appears that one side of the toxin is masked by binding to the pore, but $Lys^{17}$ is exposed to an aqueous cavity accessible to entering ions (50). As noted by Hui *et al.* (48), GIIIA therefore differs from other ion channel inhibitors such as the charybdotoxin family of $K^+$ channel blockers and the $Na^+$ channel-blocking guanidinium toxins, which appear to occlude the narrow part of the pore. Charybdotoxin (51), agitoxin-2 (52), and the sea anemone toxin ShK (53) have been shown to dock in the pore-vestibule region of the $K^+$ channel to inhibit ionic current, and tetrodotoxin and saxitoxin block at the selectivity filter (54) of a variety of $Na^+$ channels.

As discussed above, the structure of SmIIIA resembles those of GIIIA and GIIIB (and probably PIIIA) in its C-terminal half and PIIIA in its N-terminal region. The surface of SmIIIA shown in the *lower part* of Fig. 6 consists mainly of conserved Cys and Arg/Lys residues and is likely to be similar to that of PIIIA except for the presence of $Arg^8$ and $Asp^{18}$ in place of Hyp. On the other face (*upper part* of Fig. 6) the $Trp^{15}$ side chain, which is unique to SmIIIA, protrudes from the surface and is flanked by the side chains of $His^{19}$ and $Arg^2$, both of which are present in PIIIA. Other differences on this face of the molecule are $Asn^6$, $Gly^7$, and $Ser^{12}$ (Gly, Phe, and Arg, respectively, in PIIIA), while $Asp^{18}$ is at the edge (PIIIA contains no acidic residues). We believe that at least some of the residues on this face contribute to the affinity of SmIIIA for TTX-resistant channels. The other residue in SmIIIA that merits investigation is $Arg^{17}$, which replaces Lys in the other μ-conotoxins. Although the charge is the same, Arg is a bulkier side chain, and in the case of the $K^+$-channel ShK toxin, where $Lys^{22}$ inserts into the pore of the channel (53, 55), substitution with Arg reduces $K^+$-channel binding significantly (56).

Consistent with these inferences from the structure, construction and assay of two chimeras of SmIIIA and PIIIA in which their N- and C-terminal halves were recombined indicated that residues in the C-terminal half of SmIIIA confer affinity for TTX-resistant VGSCs. Substitution of the last 9 residues of PIIIA with the corresponding 10 residues from SmIIIA confers affinity for TTX-resistant VGSCs. Conversely, substitution of the last 10 residues in SmIIIA with the corresponding 9 residues from PIIIA abolishes the affinity of SmIIIA for TTX-resistant VGSCs.

In addition to determining the structure of SmIIIA and defining some of the determinants of its selectivity for TTX-resistant VGSCs, we have also further characterized its activity. Although SmIIIA inhibits TTX-resistant currents in voltage-clamped sympathetic neurons, it does not have any significant effect, by itself, on CAPs in the postganglionic axons of these neurons (data not shown), confirming that the TTX-sensitive VGSCs expressed in these neurons are largely resistant to SmIIIA. The manifestation of the inhibition of TTX-resistant VGSCs by SmIIIA is only unmasked when TTX-sensitive channels are functionally removed from these axons by prior application of TTX. When this is done, both SmIIIA and the P-Sm chimera inhibit C-neuron CAPs that persist in 10 μM TTX. This indicates that the axons of C-neurons express sufficient levels of both TTX-sensitive and TTX-resistant VGSCs to allow action potentials to be propagated in the absence of either (but not both) types of channels.

*Acknowledgments*—We thank Edward Grixti for assistance with spectral acquisition, Jennifer Sabo for measurement of temperature coefficients, and Peter Güntert for helpful advice on the use of CANDID. We also thank Jacob Nielsen and Olga Buczek for preparation of the synthetic peptides.

REFERENCES

1. Olivera, B. M., Hillyard, D. R., Marsh, M., and Yoshikami, D. (1995) *Trends Biotechnol.* **13,** 422–426
2. Jones, R. M., and Bulaj, G. (2000) *Curr. Pharm. Des.* **6,** 1249–1285

3. Cestele, S., and Catterall, W. A. (2000) *Biochimie (Paris)* **82,** 883–892
4. Goldin, A. L. (2001) *Annu. Rev. Physiol.* **63,** 871–894
5. Catterall, W. A. (2000) *Neuron* **26,** 13–25
6. Cruz, L. J., Gray, W. R., Olivera, B. M., Zeikus, R. D., Kerr, L., Yoshikami, D., and Moczydlowski, E. (1985) *J. Biol. Chem.* **260,** 9280–9288
7. Moczydlowski, E., Olivera, B. M., Gray, W. R., and Strichartz, G. R. (1986) *Proc. Natl. Acad. Sci. U. S. A.* **83,** 5321–5325
8. Safo, P., Rosenbaum, T., Shcherbatko, A., Choi, D. Y., Han, E., Toledo-Aral, J. J., Olivera, B. M., Brehm, P., and Mandel, G. (2000) *J. Neurosci.* **20,** 76–80
9. Li, R. A., Ennis, I. L., Xue, T., Nguyen, H. M., Tomaselli, G. F., Goldin, A. L., and Marban, E. (2003) *J. Biol. Chem.* **278,** 8717–8724
10. Chen, L. Q., Chahine, M., Kallen, R. G., Barchi, R. L., and Horn, R. (1992) *FEBS Lett.* **309,** 253–257
11. Ohizumi, Y., Nakamura, H., Kobayashi, J., and Catterall, W. A. (1986) *J. Biol. Chem.* **261,** 6149–6152
12. Shon, K. J., Olivera, B. M., Watkins, M., Jacobsen, R. B., Gray, W. R., Floresca, C. Z., Cruz, L. J., Hillyard, D. R., Brink, A., Terlau, H., and Yoshikami, D. (1998) *J. Neurosci.* **18,** 4473–4481
13. Nielsen, K. J., Watson, M., Adams, D. J., Hammarstrom, A. K., Gage, P. W., Hill, J. M., Craik, D. J., Thomas, L., Adams, D., Alewood, P. F., and Lewis, R. J. (2002) *J. Biol. Chem.* **277,** 27247–27255
14. West, P. J., Bulaj, G., Garrett, J. E., Olivera, B. M., and Yoshikami, D. (2002) *Biochemistry* **41,** 15388–15393
15. Lancelin, J. M., Kohda, D., Tate, S., Yanagawa, Y., Abe, T., Satake, M., and Inagaki, F. (1991) *Biochemistry* **30,** 6908–6916
16. Ott, K. H., Becker, S., Gordon, R. D., and Rüterjans, H. (1991) *FEBS Lett.* **278,** 160–166
17. Wakamatsu, K., Kohda, D., Hatanaka, H., Lancelin, J. M., Ishida, Y., Oya, M., Nakamura, H., Inagaki, F., and Sato, K. (1992) *Biochemistry* **31,** 12577–12584
18. Hill, J. M., Alewood, P. F., and Craik, D. J. (1996) *Biochemistry* **35,** 8824–8835
19. Miles, L. A., Dy, C. Y., Nielsen, J., Barnham, K. J., Hinds, M. G., Olivera, B. M., Bulaj, G., and Norton, R. S. (2002) *J. Biol. Chem.* **277,** 43033–43040
20. Piotto, M., Saudek, V., and Sklenar, V. (1992) *J. Biomol. NMR* **2,** 661–665
21. Bartels, C., Xia, T. H., Billeter, M., Güntert, P., and Wüthrich, K. (1995) *J. Biomol. NMR* **6,** 1–10
22. Seavey, B. R., Farr, E. A., Westler, W. M., and Markley, J. L. (1991) *J. Biomol. NMR* **1,** 217–236
23. Ludvigsen, S., and Poulsen, F. M. (1992) *J. Biomol. NMR* **2,** 227–233
24. Herrmann, T., Güntert, P., and Wüthrich, K. (2002) *J. Mol. Biol.* **319,** 209–227
25. Schwieters, C. D., Kuszewski, J. J., Tjandra, N., and Clore, G. M. (2003) *J. Magn. Reson.* **160,** 65–73
26. Laskowski, R. A., Rullmannn, J. A., MacArthur, M. W., Kaptein, R., and Thornton, J. M. (1996) *J. Biomol. NMR* **8,** 477–486
27. Koradi, R., Billeter, M., and Wüthrich, K. (1996) *J. Mol. Graph.* ***14,*** 29–32; 51–55
28. Nicholls, A., Sharp, K. A., and Honig, B. (1991) *Proteins* **11,** 281–296
29. Jones, S. W. (1987) *J. Physiol. (Lond.)* **389,** 605–627
30. Selyanko, A. A., Smith, P. A., and Zidichouski, J. A. (1990) *J. Physiol. (Lond.)* **425,** 471–500
31. Tavazoie, S. F., Tavazoie, M. F., McIntosh, J. M., Olivera, B. M., and Yoshikami, D. (1997) *Br. J. Pharmacol.* **120,** 995–1000
32. Baxter, N. J., and Williamson, M. P. (1997) *J. Biomol. NMR* **9,** 359–369
33. Berman, H. M., Battistuz, T., Bhat, T. N., Bluhm, W. F., Bourne, P. E., Burkhardt, K., Feng, Z., Gilliland, G. L., Iype, L., Jain, S., Fagan, P., Marvin, J., Padilla, D., Ravichandran, V., Schneider, B., Thanki, N., Weissig, H., Westbrook, J. D., and Zardecki, C. (2002) *Acta Crystallogr. Sect. D Biol. Crystallogr.* **58,** 899–907
34. Burley, S. K., and Petsko, G. A. (1986) *FEBS Lett.* **203,** 139–143
35. Syed, R. S., Reid, S. W., Li, C., Cheetham, J. C., Aoki, K. H., Liu, B., Zhan, H., Osslund, T. D., Chirino, A. J., Zhang, J., Finer-Moore, J., Elliott, S., Sitney, K., Katz, B. A., Matthews, D. J., Wendoloski, J. J., Egrie, J., and Stroud, R. M. (1998) *Nature* **395,** 511–516
36. Case, D. A. (1995) *J. Biomol. NMR* **6,** 341–346
37. Keim, P., Vigna, R. A., Morrow, J. S., Marshall, R. C., and Gurd, F. R. N. (1973) *J. Biol. Chem.* **248,** 7811–7818
38. Bundi, A., and Wüthrich, K. (1979) *Biopolymers* **18,** 285–297
39. Tanokura, M., Tasumi, M., and Miyazawa, T. (1976) *Biopolymers* **15,** 393–401
40. Perutz, M. F., Gronenborn, A. M., Clore, G. M., Fogg, J. H., and Shih, D. T. (1985) *J. Mol. Biol.* **183,** 491–498
41. Shire, S. J., Hanania, G. I., and Gurd, F. R. N. (1974) *Biochemistry* **13,** 2967–2974
42. Smith, P. A. (1994) *Prog. Neurobiol.* **43,** 439–510
43. Sato, K., Ishida, Y., Wakamatsu, K., Kato, R., Honda, H., Ohizumi, Y., Nakamura, H., Ohya, M., Lancelin, J. M., Kohda, D., and Inagaki, F. (1991) *J. Biol. Chem.* **266,** 16989–16991
44. Becker, S., Prusak-Sochaczewski, E., Zamponi, G., Beck-Sickinger, A. G., Gordon, R. D., and French, R. J. (1992) *Biochemistry* **31,** 8229–8238
45. Chahine, M., Chen, L.-Q., Fotouhi, N., Walsky, R., Fry, D., Santarelli, V., Horn, R., and Kallen, R. G. (1995) *Receptors Channels* **3,** 161–174
46. Dudley, S. C., Jr., Todt, H., Lipkind, G., and Fozzard, H. A. (1995) *Biophys. J.* **69,** 1657–1665
47. French, R. J., Prusak-Sochaczewski, E., Zamponi, G. W., Becker, S., Kularatna, A. S., and Horn, R. (1996) *Neuron* **16,** 407–413
48. Hui, C., Goto, A., Yamada, K., Yagi, N., Nagoshi, H., Sasabe, M., and Omata, M. (1996) *Life Sci.* **58,** 359–366
49. Li, R. A., Sato, K., Kodama, K., Kohno, T., Xue, T., Tomaselli, G. F., and Marban, E. (2002) *FEBS Lett.* **511,** 159–164
50. Hui, K., Lipkind, G., Fozzard, H. A., and French, R. J. (2002) *J. Gen. Physiol.* **119,** 45–54
51. Miller, C. (1995) *Neuron* **15,** 5–10
52. MacKinnon, R., Cohen, S. L., Kuo, A., Lee, A., and Chait, B. T. (1998) *Science* **280,** 106–109
53. Lanigan, M. D., Kalman, K., Lefievre, Y., Pennington, M. W., Chandy, K. G., and Norton, R. S. (2002) *Biochemistry* **41,** 11963–11971
54. Hille, B. (2001) *Ion channels in Excitable Membranes*, 3rd Ed., Sinauer Associates, Sunderland, MA
55. Kalman, K., Pennington, M. W., Lanigan, M. D., Nguyen, A., Rauer, H., Mahnir, V., Paschetto, K., Kem, W. R., Grissmer, S., Gutman, G. A., Christian, E. P., Cahalan, M. D., Norton, R. S., and Chandy, K. G. (1998) *J. Biol. Chem.* **273,** 32697–32707
56. Pennington, M. W., Mahnir, V. M., Krafte, D. S., Zaydenberg, I., Byrnes, M. E., Khaytin, I., Crowley, K., and Kem, W. R. (1996) *Biochem. Biophys. Res. Commun.* **219,** 696–701